

CHAPTER FIVE

DETECTING LAND-COVER CHANGE USING MODIS TIME-SERIES DATA

5.1 INTRODUCTION

In this chapter two novel change detection methods are proposed. The first method, hereafter referred to as the EKF change detection method, is based on the work done in the previous chapter. The algorithm acts as a per-pixel change alarm and takes as input the NDVI time-series of a 3×3 grid of MODIS pixels. The NDVI time-series for each of these pixels was modeled as a triply (mean, phase and amplitude) modulated cosine function, and an EKF was used to estimate the parameters of the modulated cosine function for each time-step. A spatial comparison between the center pixel of the the 3×3 grid and each of its neighboring pixel's mean and amplitude parameter sequence was done to calculate a change metric. This change metric is then compared to a threshold to yield a change or no-change decision.

The second method, hereafter referred to as the temporal ACF change detection method, is a per-pixel change alarm that uses temporal autocorrelation to infer a change metric which also yields a change or no-change decision after thresholding.

A third method, which is based on the work of Lunetta et al. [17] (see section 2.7.1.3), is also shown in this chapter. This method uses a MODIS NDVI time-series to determine the occurrence of change in areas that are typically covered by natural vegetation and was included for comparison. All three these methods were compared with one another and their results are presented in chapter 6.

Both of the proposed methods (EKF and ACF change detection methods) make use of a simulated change dataset for initial parameter estimation. Making use of simulated or synthetic data is a

well-known concept in the remote sensing community [25, 97, 98]. The use of simulated change data is twofold. Firstly, during development of the new method the simulated change data were used to optimize the method and to tentatively evaluate the performance of the algorithm. Simulation was opted for during the optimization phase, since new settlement developments are infrequently mapped on an ad hoc basis in South Africa and the data on known settlement development amount to a relatively small number of MODIS pixels. Secondly, the start date and rate of the land-cover change could be controlled in the simulated or synthetic data which greatly facilitates the development and evaluation phases. After the method was optimized and performing well on simulated (synthetic) change data, it was evaluated by applying it to examples of known new settlement developments in South Africa.

5.2 EKF CHANGE DETECTION METHOD

Based on the results obtained in the previous chapter, the focus in this chapter shifts towards land-cover change detection. In the previous chapter it was shown that a triply modulated cosine function can be used to model an NDVI time-series and that the parameters of the function can be estimated for each time-step using a non-linear EKF. The consequent μ and α parameter stream is expected to be similar for the same class land-cover types and dissimilar for different land-cover types when considering natural vegetation and settlement pixels. Assuming that land-cover separability is achievable, it can be inferred that when a land-cover type changes from a naturally vegetated state to a settlement state, the corresponding μ and α parameter sequence will also be affected. The proposed method uses a MODIS 8-day NDVI time-series (see section 2.18) to calculate a change metric by means of a spatial comparison of the EKF parameter sequence of any given pixel with that of its neighboring pixels. The objective was to demonstrate that by making use of an EKF-derived change metric and a threshold optimized based on simulated land-cover change, a semi-supervised change detection method can be formulated that accurately detects change using MODIS NDVI time-series data.

5.2.1 Change metric formulation

As was shown in chapter 4, the NDVI time-series for a given pixel can be modeled by a triply modulated cosine function given as

$$y_k = \mu_k + \alpha_k \cos(\omega k + \phi_k) + v_k, \quad (5.1)$$

where y_k denotes the observed value of the NDVI time-series at time k and v_k is the noise sample at time k . The values of μ_k , α_k and ϕ_k are functions of time, and must be estimated given y_k for

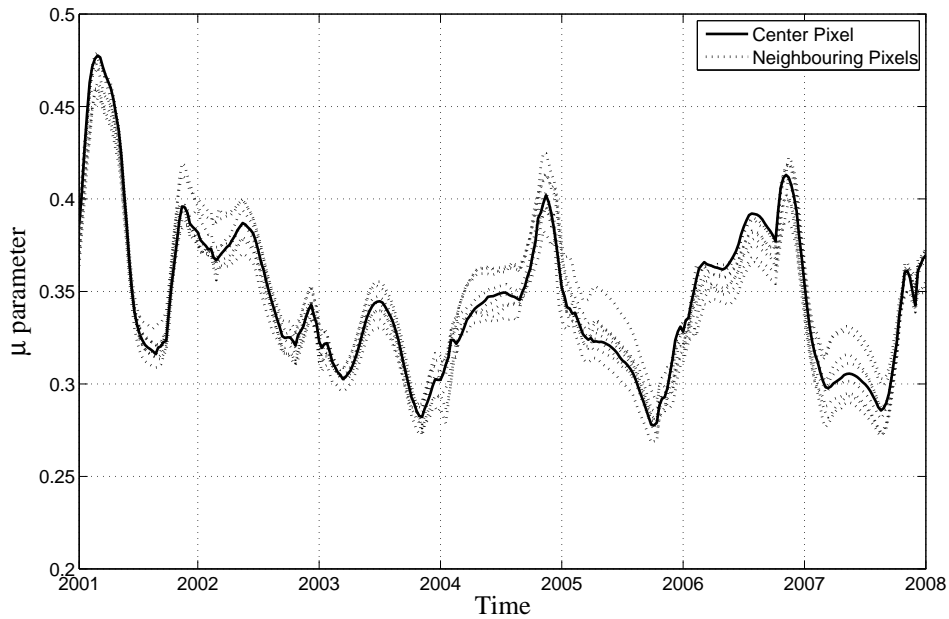


FIGURE 5.1: Mean parameter sequence comparison of a 3×3 pixel grid having an unchanged center pixel.

$k \in 1, \dots, N$ [99, 100]. An EKF was used to estimate these parameters for every increment of k . The estimated values for $\mathbf{x}_k = [\mu_k \alpha_k \phi_k]^T$ over time k effectively results in a time-series for each of the three parameters.

Having the parameter sequence for μ_k , α_k and ϕ_k for $k \in 1, \dots, N$ for a given pixel, a change detection method was formulated by comparing the parameter sequences of the pixel with that of its direct neighboring pixels. This effectively means focusing on the center pixel of a 3×3 grid of pixels and examining each neighboring pixel's EKF parameter sequence relative to the center pixel. It was found that the ϕ parameter sequence does not yield any significant separability between natural vegetation and settlement land-cover types and consequently only the μ and α parameter sequences were considered (See section 6.2.2).

Figure 5.1 shows the μ parameter sequence of a natural vegetation pixel over the seven-year study period compared to that of its neighboring pixels. As expected, the μ parameter sequence for the nine pixels is highly correlated. Figure 5.2 shows the μ parameter sequence for the same grid but with the center pixel gradually changing to settlement over a 6 month period. It is clear that the μ parameter sequence for the center pixel becomes less correlated with that of its neighboring pixels. The μ and α parameter sequence difference between the center pixel and an arbitrary neighboring pixel at time k

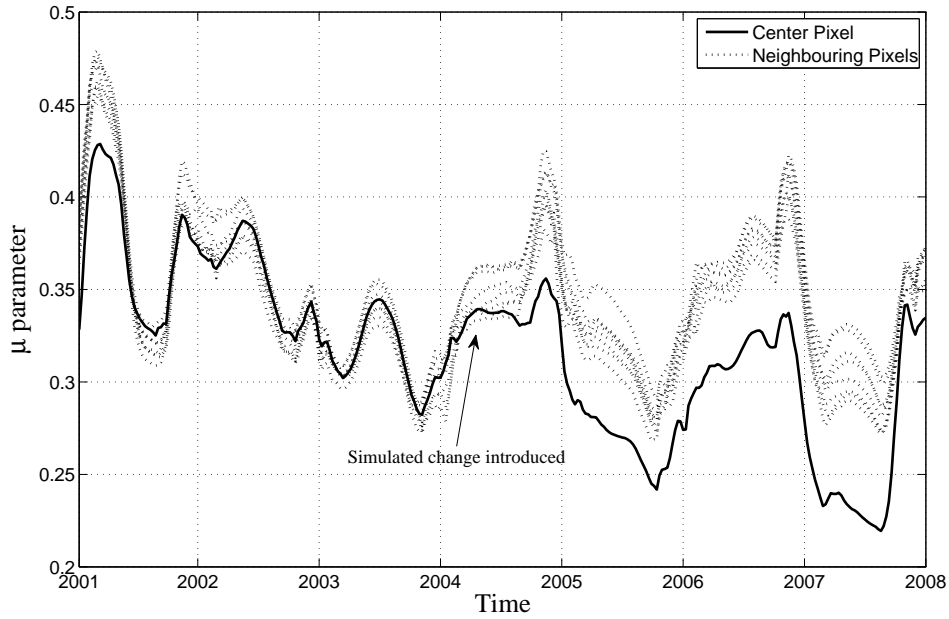


FIGURE 5.2: Mean parameter sequence comparison of a 3×3 pixel grid with simulated natural vegetation to settlement change introduced to the center pixel.

can be written as

$$D_{\mu(n)}^k = |\mu_k - \mu_k^n| \quad n \in 1, \dots, 8, \quad (5.2)$$

$$D_{\alpha(n)}^k = |\alpha_k - \alpha_k^n| \quad n \in 1, \dots, 8, \quad (5.3)$$

where $D_{\mu(n)}^k$ is the distance between the μ parameter sequence of a selected pixel (μ_k) with its n th neighboring pixel (μ_k^n) at time k . $D_{\alpha(n)}^k$ is the distance between the α parameter sequence of a selected pixel (α_k) with its n th neighboring pixel (α_k^n) at time k . Equation 5.2 and 5.3 can be combined as

$$D_n^k = D_{\mu(n)}^k + D_{\alpha(n)}^k \quad n \in 1, \dots, 8. \quad (5.4)$$

Having obtained the distance of the center pixel's parameter sequences relative to each of the neighboring pixel's parameter sequences, these could be combined at time k by simply adding all the values of $D_n^k \quad n \in 1, \dots, 8$ at time k

$$D^k = \sum_{n=1}^8 D_n^k \quad k \in 1, \dots, N. \quad (5.5)$$

Having vector $\mathbf{D} = [D^1 \ D^2 \ D^3 \ \dots \ D^N]$, a change metric was derived by firstly determining how the relative distance of the parameter sequences between the center pixel and its neighboring pixel changes

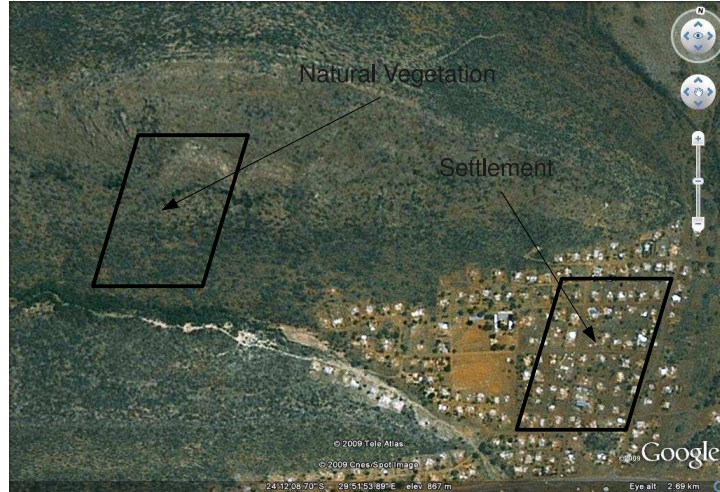


FIGURE 5.3: 500 m MODIS pixel covering natural vegetation and settlement land-cover in close proximity (courtesy of GoogleTMEarth).

through time. This was done by differentiating the vector D . A single change metric was then derived by summing all the values of the differentiated D vector to yield

$$\delta = \sum_{k=2}^N |D^k - D^{k-1}|, \quad (5.6)$$

where δ is a single valued change metric for the center pixel of the 3×3 pixel grid. The change metric for each of the pixels in the study area was thus calculated by sliding a 3×3 pixel grid over the entire study area and calculating δ for the center pixel in each case.

5.2.2 Off-line optimization phase

Simulated change data are used together with a no-change dataset to optimize and tentatively evaluate the change detection method. Simulated change data were created by linearly blending a time-series of a pixel covered by natural vegetation with that of a pixel of a settlement which is in close proximity to ensure that the rainfall, soil type and local climate was similar. Figure 5.3 shows the footprint of a typical MODIS pixel covered by natural vegetation and a settlement pixel in close proximity. Figure 5.4 shows the corresponding NDVI time-series from 2001/01 to 2008/01 for each of these pixels as well as the simulated time-series where the blending period was set at 6, 12 and 24 months respectively with the midpoint of the blending period being 2004/04. It was found that the method was not sensitive to the exact date of change but rather to the transition duration, hence the variable simulated blending period. As was discussed in section 5.2.1, the algorithm uses a 3×3 pixel grid with the center pixel being compared to all neighboring pixels. It is, however, not realistic to assume that only the center pixel has changed with all neighboring pixels remaining unchanged. For this reason,

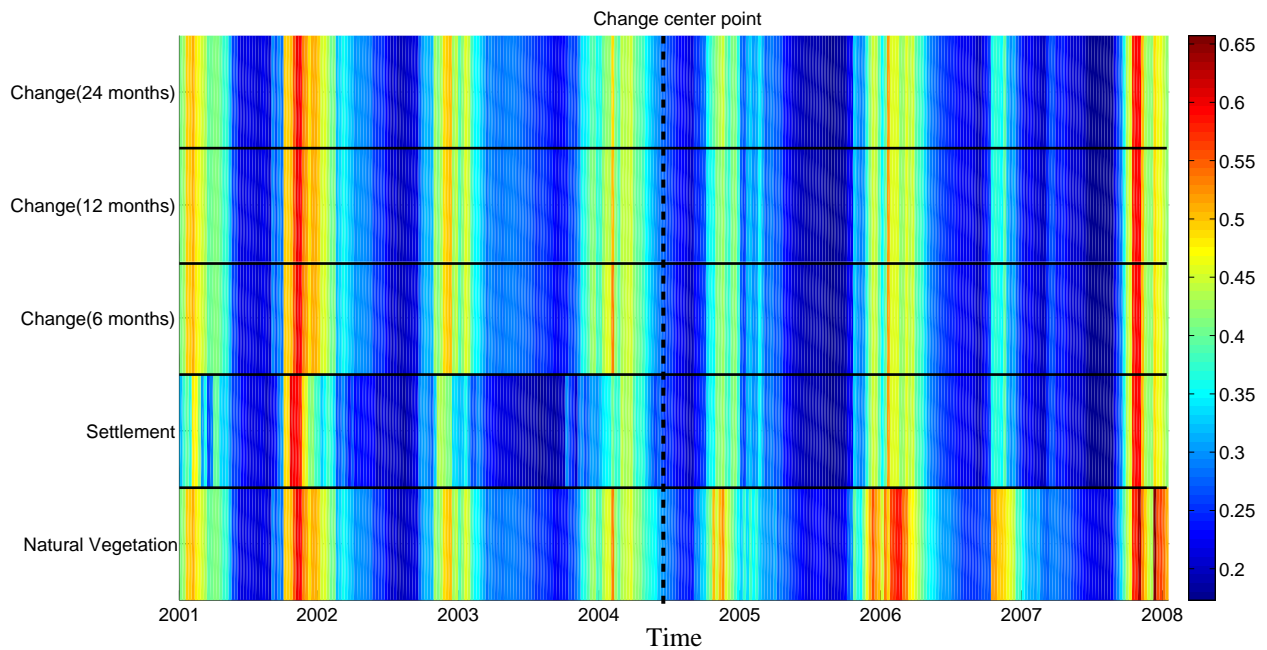


FIGURE 5.4: NDVI time-series of natural vegetation, settlement and simulated change pixels where the simulated change time-series had blending periods of 6, 12 and 24 months respectively.

the center pixel, together with a subset of neighboring pixels (zero to all eight), were subjected to a simulated land-cover change. The simulated change for each of the neighboring pixels was done in a similar manner, ensuring that the initial state of each neighboring pixel is in a vegetated state and gradually blends to a settlement state.

As previously stated, the method requires an *a-priori* database of simulated change and no-change examples. The change metric is firstly calculated (equation 5.6) for all the no-change and simulated change pixels in the database. The distribution of δ for both cases is then calculated. Figure 5.5 shows an example of the anticipated distribution of δ in the case of no-change $p(\delta|\bar{C})$ and simulated change $p(\delta|C_r^p)$ respectively. In $p(\delta|C_r^p)$, r is the rate of simulated change, i.e. 6, 12 or 24 months and p is the number of pixels in the 3×3 grid subjected to a simulated change. The value of the optimal threshold (δ^*) will change depending on the value of p and r respectively. The Bayesian decision error can be calculated as

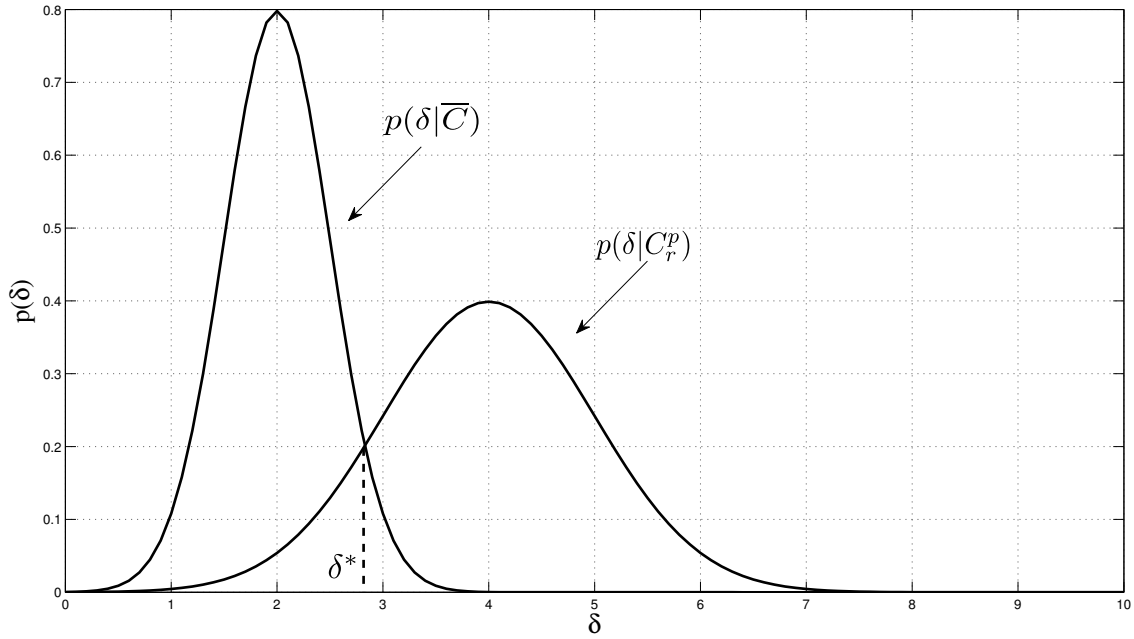


FIGURE 5.5: Probability distribution of δ in the case of no-change $p(\delta|\bar{C})$ and simulated change $p(\delta|C_r^p)$ respectively.

$$P(C|C) = \int_{\delta=\delta^*}^{\delta=\infty} p(\delta|C_r^p), \quad (5.7)$$

$$P(C|\bar{C}) = \int_{\delta=\delta^*}^{\delta=\infty} p(\delta|\bar{C}), \quad (5.8)$$

$$P(\bar{C}|C) = \int_{\delta=0}^{\delta=\delta^*} p(\delta|C_r^p), \quad (5.9)$$

$$P(\bar{C}|\bar{C}) = \int_{\delta=0}^{\delta=\delta^*} p(\delta|\bar{C}). \quad (5.10)$$

$P(C|C)$ is the probability that a change was detected given that a change was introduced (percentage change correctly detected), $P(C|\bar{C})$ is the probability that a change was detected given that no change was introduced (percentage false alarms), $P(\bar{C}|C)$ is the probability that no change was detected given that a change was introduced and $P(\bar{C}|\bar{C})$ is the probability that no change was detected given that no change was introduced (5.7)-(5.10). The value of δ^* is the optimal decision threshold that minimizes the Bayesian decision error.

The underlying idea is that $p(\delta|\bar{C})$, which is estimated using actual no-change examples, remains constant, while $p(\delta|C_r^p)$ which is estimated using simulated change data varies for different realizations of p and r . This implies that that δ^* will vary for different values of r and p . By calculating δ^* for all

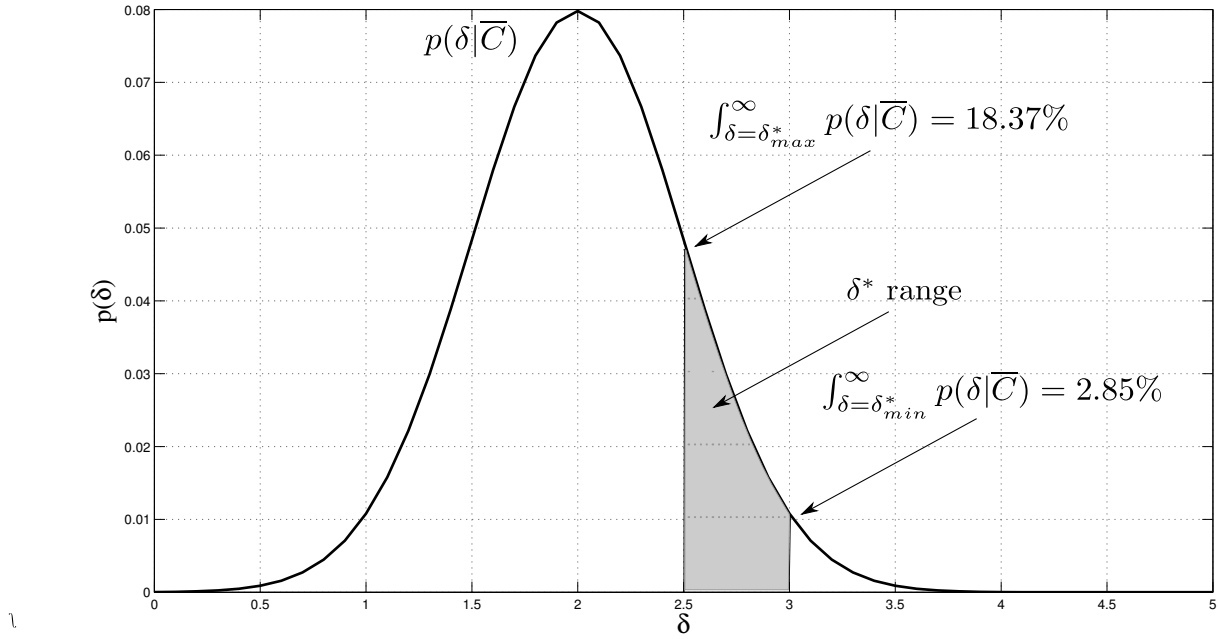


FIGURE 5.6: Range of δ^* and corresponding maximum and minimum false alarm rate.

values of $r \in \{6, 12, 24\}$ and $p = \{1, 2, 3, \dots, 9\}$, will result in a range of δ^* values. Each of the δ^* values in this range result in a different false alarm rate, calculated using $p(\delta|\bar{C})$. Figure 5.6 shows an example of $p(\delta|\bar{C})$, together with a range of δ^* , which was determined by means of simulated change with all permutations of $r \in \{6, 12, 24\}$ and $p = \{1, 2, 3, \dots, 9\}$. The corresponding maximum and minimum false alarm rate is also shown. Having a range of false alarm rates that were identified as being optimal for different change scenarios, it is up to the operator to select the maximum allowable false alarm rate that is deemed acceptable in the given application environment.

5.2.3 Operational phase

The threshold that is selected for operational use ($\hat{\delta}$) is within the range $[\delta_{min}^*, \delta_{max}^*]$ and corresponds to the maximum allowable false alarm rate (Δ) chosen by an operator for the specific application and region. The δ^* value corresponding to Δ ($\hat{\delta}$) is expressed as:

$$\hat{\delta} = \delta^* \text{ where } \int_{\delta=\delta^*}^{\delta=\infty} p(\delta|\bar{C}) = \Delta \quad \delta^* \in [\delta_{min}^*, \delta_{max}^*]. \quad (5.11)$$

Having the value of $\hat{\delta}$, the EKF change detection method is run in an unsupervised manner for the entire study area. The value of δ (equation 5.6) is calculated for each pixel and a change is declared if δ exceeds the threshold value $\hat{\delta}$

$$\text{Change} = \begin{cases} \text{true} & \text{if } \delta \geq \hat{\delta} \\ \text{false} & \text{if } \delta < \hat{\delta}. \end{cases}$$

For example, if the no-change PDF corresponded to the one shown in Figure 5.6, the region of the optimal false alarm rate would be between 2.85% and 13.37%, which corresponds to a δ^* value of 3 and 2.5 respectively. An operator thus needs to choose the maximum allowable false alarm rate within the aforementioned range. If the maximum false alarm rate chosen by the operator was 10%, the corresponding value of δ^* could easily be determined as being 2.65, in which case:

$$\text{Change} = \begin{cases} \text{true} & \text{if } \delta \geq 2.65 \\ \text{false} & \text{if } \delta < 2.65. \end{cases}$$

5.3 TEMPORAL ACF METHOD

The ACF, in the temporal context, have been used selectively in remote sensing [101], but is mostly applied in the spatial context [102], [103]. In this section the temporal ACF of a pixel's time-series was considered. An ACF of a time-series that is stationary behaves differently from an ACF of a time-series that is non-stationary due to land-cover change. It should be noted that the ACF of a non-stationary time-series under the ergodic assumption can not be technically defined as being the ACF of the time-series. When referring to the ACF in this context, it only refers to the ACF operation performed on the given time-series under the assumption that the time-series is stationary. By determining suitable detection parameters using only a no-change database, it will be shown that real land-cover change can be detected reliably in a semi-supervised fashion.

Similar to the EKF change detection method, the temporal ACF change detection method uses a two-stage approach. Firstly, a simulated change dataset, together with a no-change dataset, is used in an off-line optimization phase to determine the appropriate parameters (band, lag and threshold selection). Second, the method is run in an unsupervised manner using the parameter-set that was determined during the aforementioned off-line optimization phase. These two stages will be discussed in further detail in the following sections.

5.3.1 Change metric formulation

Assume that the time-series for any given band of MODIS is expressed as:

$$X_n^b \quad n \in \{1, 2, \dots, N\} \quad b \in \{1, 2, \dots, 8\}, \quad (5.12)$$

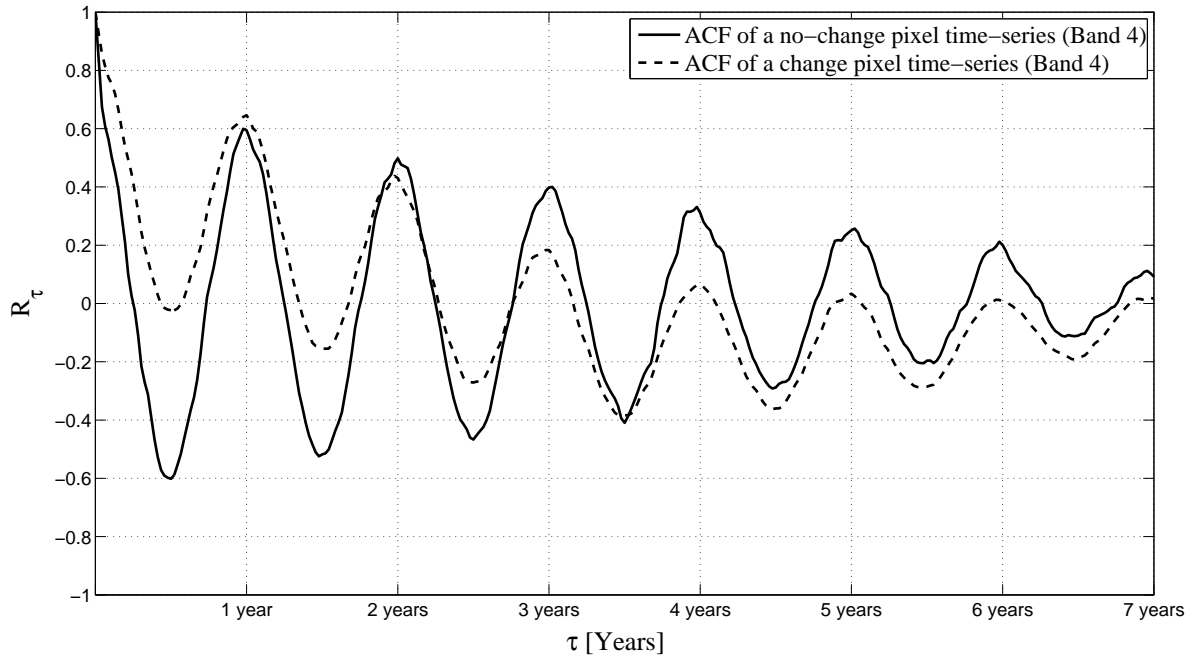


FIGURE 5.7: Autocorrelation of a change and no-change pixel's MODIS band 4 time-series.

where X_n^b is the observation from spectral band b at time n and N is the number of time-series observations available. It should be noted that band 8 in (5.12) refers to computed NDVI. It is assumed that N is equal for all seven bands.

The normalized ACF for time-series $\mathbf{X}^b = [X_1^b, X_2^b, \dots, X_N^b]$ can then be expressed as:

$$R^b(\tau) = \frac{E[(X_n^b - \mu^b)(X_{n+\tau}^b - \mu^b)]}{\text{var}(\mathbf{X}^b)}, \quad (5.13)$$

where τ is the time-lag and E denotes the expectation. The mean of \mathbf{X}^b is given as μ^b and the variance, which is used for normalization, is given as $\text{var}(\mathbf{X}^b)$. Figure 5.7 shows the typical ACF of an actual change and no-change pixel's time-series. It is clear that the no-change pixel has a symmetrical form relative to the $R^b(\tau) = 0$ axis, whereas the change pixel shows a strong non-symmetrical property. The reason for this is the stationarity requirement of the ACF in (5.13). The mean and variance of the time-series of X_n^b in (5.13) is required to remain constant through time to determine the true ACF of the time-series. The inconsistency of the mean and variance typically associated with a change pixel's non-stationary time-series thus becomes apparent when analyzing the ACF of the time-series. The change metric is thus simply equivalent to the temporal correlation of a specific band (b) at a specific lag (τ)

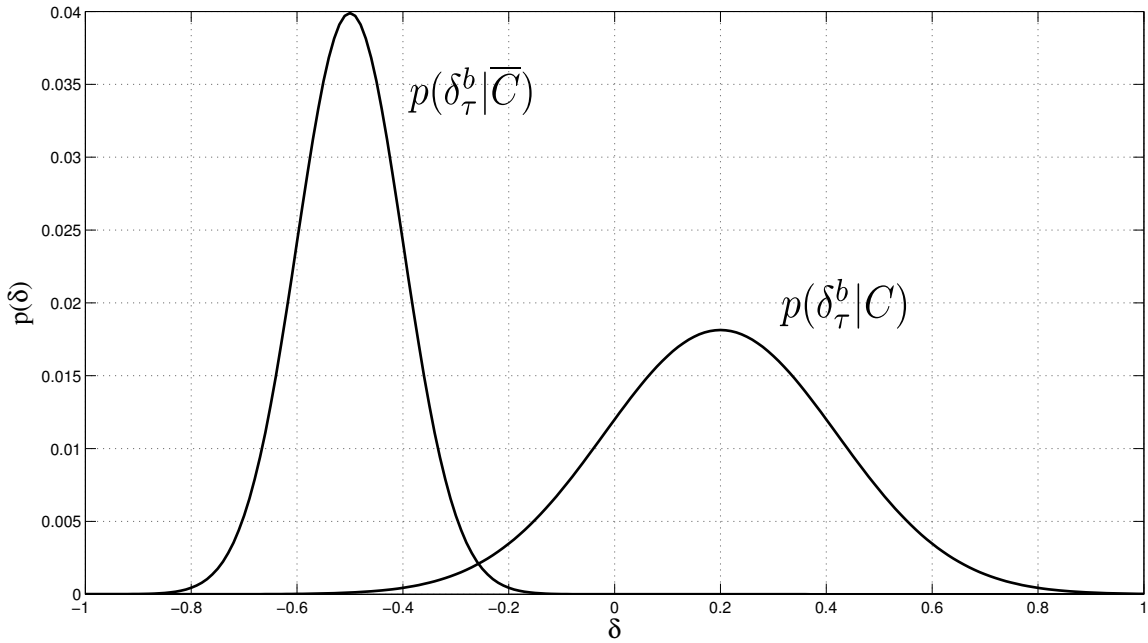


FIGURE 5.8: Example of the distribution of δ_τ^b in the case of change and no-change respectively.

$$R^b(\tau) = \delta_\tau^b. \quad (5.14)$$

It is clear, however, that the distribution of δ_τ^b in the case of change and no-change, as shown in figure 5.8, will vary for different values of τ and b . The aim is thus to determine the value of τ and b in δ_τ^b that will result in the most separable distributions between δ_τ^b for the change ($p(\delta_\tau^b|C)$) and no-change ($p(\delta_\tau^b|\bar{C})$) case respectively. The value of the optimal threshold (δ_τ^{b*}) also needs to be determined. The selection procedure for these parameters are done in an off-line optimization phase and will be discussed in more detail in the following section.

5.3.2 Off-line optimization phase

Similar to the methodology used in section 5.2.2, a no-change and simulated change dataset is used to optimize the parameters of the temporal ACF change detection method. A simulated change dataset is generated by linearly blending a time-series of a pixel covered by natural vegetation with that of a settlement pixel time-series. Unlike the simulated change dataset used in section 5.2.2, the start date of change is chosen at random. The resulting simulated change database thus has a uniformly spread change date between 2001/01 and 2008/01 corresponding to the study period. The blending period was found not to influence the method's performance, and a representative blending period of

6 months was chosen.

The right sided normalized ACF for band b can be expressed as $R^b(\tau) = [R^b(0), R^b(1), \dots, R^b(N)]$. The task at hand is to determine the separation between the ACF of the change and no-change dataset for each band at each lag. The Bayesian decision error in the form of a confusion matrix was calculated based on the distribution of the change metric δ_τ^b for the change and no-change dataset:

$$P(C|C) = \int_{\delta_\tau^b = \delta_\tau^{b*}}^{\delta_\tau^b = \infty} p(\delta_\tau^b|C), \quad (5.15)$$

$$P(C|\bar{C}) = \int_{\delta_\tau^b = \delta_\tau^{b*}}^{\delta_\tau^b = \infty} p(\delta_\tau^b|\bar{C}), \quad (5.16)$$

$$P(\bar{C}|C) = \int_{\delta_\tau^b = 0}^{\delta_\tau^b = \delta_\tau^{b*}} p(\delta_\tau^b|C), \quad (5.17)$$

$$P(\bar{C}|\bar{C}) = \int_{\delta_\tau^b = 0}^{\delta_\tau^b = \delta_\tau^{b*}} p(\delta_\tau^b|\bar{C}). \quad (5.18)$$

$P(C|C)$ is the probability that a change was detected given that a change was present (percentage change correctly detected), $P(C|\bar{C})$ is the probability that a change was detected given that no change was present (percentage false alarms), $P(\bar{C}|C)$ is the probability that no change was detected given that a change was introduced and $P(\bar{C}|\bar{C})$ is the probability that no change was detected given that no change was introduced. The value of δ_τ^{b*} is the optimal decision threshold. To relate the confusion matrix into a single measure of accuracy, the overall accuracy was calculated as:

$$O_A = \frac{P(C|C) + P(\bar{C}|\bar{C})}{P(C|C) + P(\bar{C}|\bar{C}) + P(C|\bar{C}) + P(\bar{C}|C)}. \quad (5.19)$$

The optimal value of τ , b and δ_τ^{b*} could thus be calculated by solving

$$[\tau, b, \delta_\tau^{b*}] = \operatorname{argmax}_{\tau, b, \delta_\tau^{b*}} \frac{\int_{\delta_\tau^b = \delta_\tau^{b*}}^{\delta_\tau^b = \infty} p(\delta_\tau^b|C) + \int_{\delta_\tau^b = 0}^{\delta_\tau^b = \delta_\tau^{b*}} p(\delta_\tau^b|\bar{C})}{\int_{\delta_\tau^b = \delta_\tau^{b*}}^{\delta_\tau^b = \infty} p(\delta_\tau^b|C) + \int_{\delta_\tau^b = 0}^{\delta_\tau^b = \delta_\tau^{b*}} p(\delta_\tau^b|\bar{C}) + \int_{\delta_\tau^b = \delta_\tau^{b*}}^{\delta_\tau^b = \infty} p(\delta_\tau^b|\bar{C}) + \int_{\delta_\tau^b = 0}^{\delta_\tau^b = \delta_\tau^{b*}} p(\delta_\tau^b|C)}, \quad (5.20)$$

where $p(\delta_\tau^b|C)$ is estimated by means of the simulated change dataset and $p(\delta_\tau^b|\bar{C})$ is calculated using the no-change dataset.

5.3.3 Operational phase

After the off-line optimization phase is complete, the resulting parameters are used to run the algorithm in an unsupervised manner for the entire area of interest. A pixel is labeled as having changed by

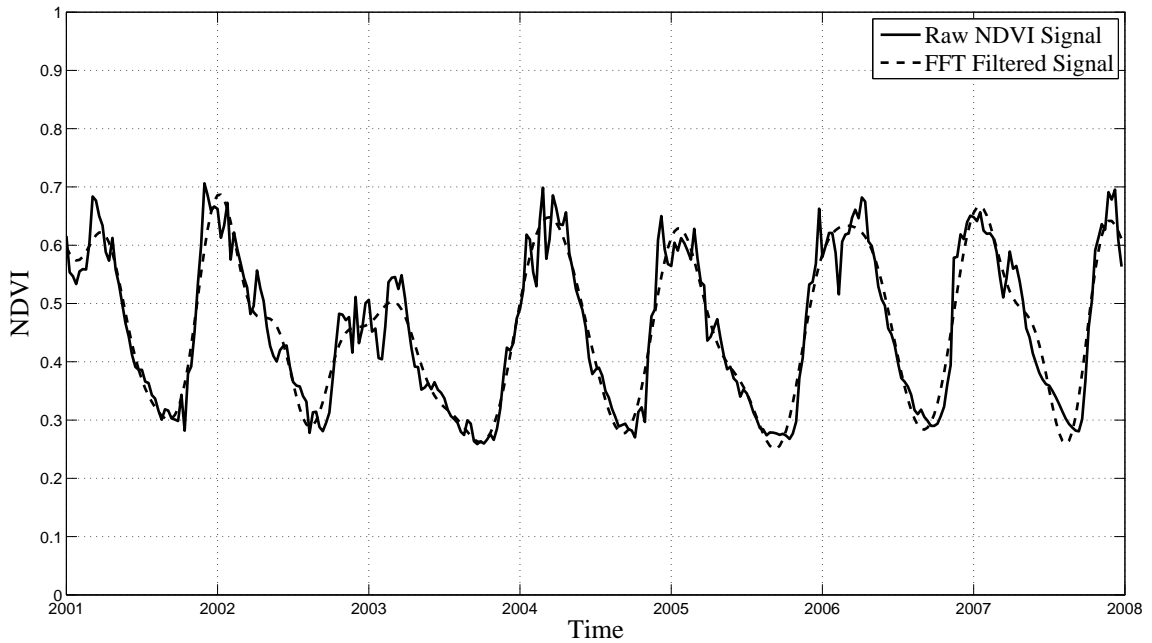


FIGURE 5.9: Comparison between a raw and filtered NDVI signal.

evaluating the following,

$$\text{Change} = \begin{cases} \text{true} & \text{if } R^b(\tau) \geq \delta_{\tau}^{b*} \\ \text{false} & \text{if } R^b(\tau) < \delta_{\tau}^{b*}, \end{cases}$$

where $R^b(\tau)$ is the ACF of band b evaluated at lag τ and δ_{τ}^{b*} is the decision threshold. The value of τ , b and δ_{τ}^{b*} , was provided in the aforementioned off-line optimization phase. The results obtained for both the off-line optimization phase and operational phase are presented in Chapter 6.

5.4 ANNUAL NDVI DIFFERENCING METHOD

Both the EKF and ACF change detection methods are compared to a computationally simple change detection method proposed by Lunetta *et al.* [17]. Using this method, the NDVI time-series was firstly filtered and cleaned using Fourier transformation filtering. In this step, the raw NDVI signal is transformed to the frequency domain using the FFT. The high frequency components are removed and the remainder is transformed back to the time-domain using the IFFT. Figure 5.9 shows the raw NDVI signal as well as the FFT filtered signal. It is clear that the filtered signal is considerably smoother than the original raw NDVI signal.

Assume that the entire time-series of the filtered NDVI time-series is denoted as

$$\mathbf{y} = [y_1, y_2, y_3, \dots, y_N], \quad (5.21)$$

where \mathbf{y} is a vector containing the filtered NDVI value for each time-step and N is the total number of observations. A new time-series can be obtained by summing all the filtered NDVI values for a year and reducing the time-series elements to the number of years.

$$\mathbf{c} = [c_1, c_2, c_3, \dots, c_K], \quad (5.22)$$

where K is number of years that the time-series spans and c_i is the cumulative NDVI for year i given as:

$$c_i = \sum_{k=1+46(i-1)}^{k=46+46(i-1)} y_k. \quad (5.23)$$

The number 46 in equation 5.23 refers to the total number of eight day observations in a single year. The difference between the c_i for consecutive years can be expressed as a vector $\mathbf{d} = [d_1, d_2, d_3, \dots, d_{K-1}]$ where d_i is calculated as:

$$d_i = c_i - c_{i+1}. \quad (5.24)$$

The value of d_i is calculated for each of the pixels in the study area, the underlying idea being that pixels experiencing a considerable reduction in NDVI will have a higher d_i value and would thus be a good indication of land-cover change. The problem, however, is identifying a suitable threshold value that when compared to d_i , produces a change or no-change decision. The threshold value would obviously also need to be adjusted for each value of i . A pixel would be flagged as having changed if any of the values of d_i exceed the threshold δ_i for $i \in [1, 2, 3, \dots, K - 1]$. A change vector could be formulated as $\zeta = \{\zeta_1, \zeta_2, \zeta_3, \dots, \zeta_{K-1}\}$ where ζ_i is defined as

$$\zeta_i = \begin{cases} 0 & \text{if } d_i \geq \delta_i \\ 1 & \text{if } d_i > \delta_i. \end{cases}$$

A change or no-change decision is made as

$$\text{Change} = \begin{cases} \text{true} & \text{if } \sum \zeta > 0 \\ \text{false} & \text{if } \sum \zeta = 0. \end{cases}$$

Where $\sum \zeta$ refers to the summation of all the values in the vector ζ given as

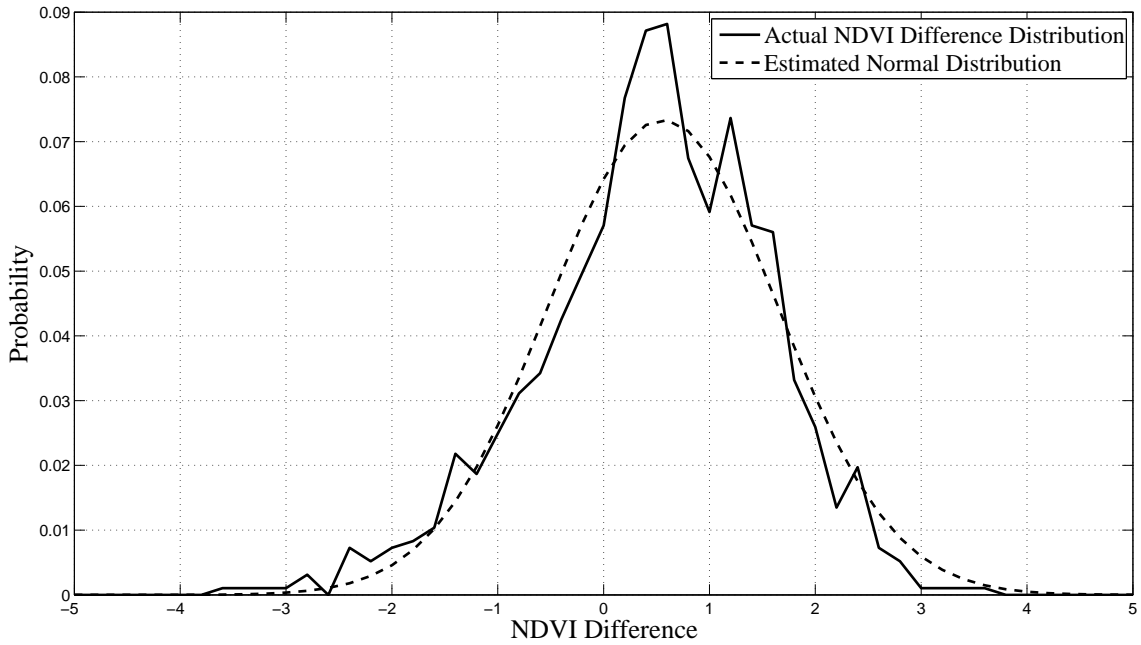


FIGURE 5.10: Distribution of the annual NDVI difference between 2002 and 2003 for the study period.

$$\sum \zeta = \sum_{i=1}^{K-1} \zeta_i. \quad (5.25)$$

Choosing the threshold values δ_i for $i \in \{1, 2, 3, \dots, K - 1\}$ is not a trivial task. This was achieved by using standard normal statistics. Firstly, the difference value (d_i , $i \in \{1, 2, 3, \dots, K - 1\}$) is computed for all the pixels in the study area. This is then used to estimate normal distribution $p(d_i)$ $i \in \{1, 2, 3, \dots, K - 1\}$. Figure 5.10 shows the annual NDVI difference between two consecutive years (2002 and 2003) during the study period. It can also be seen that the actual distribution of the NDVI difference is well approximated using a normal distribution.

Using standard normal distribution statistics, the threshold value δ_i was determined by choosing the NDVI difference value that corresponds to the z value that is representative of the *a-priori* probability of change in the study area [17]. Figure 5.11 shows a normal distribution. It can be seen that 95% of the values fall between a z value of -1.98 and 1.98 where 99% of the values are between the values of -2.58 and 2.58. It follows that if the *a-priori* change probability of 2.5% is expected for a specific area, the threshold value will correspond to a z value of 1.98 because only the right tail of the distribution is considered, as a reduction in NDVI from year to year will result in a positive d_i value when considering equation 5.24.

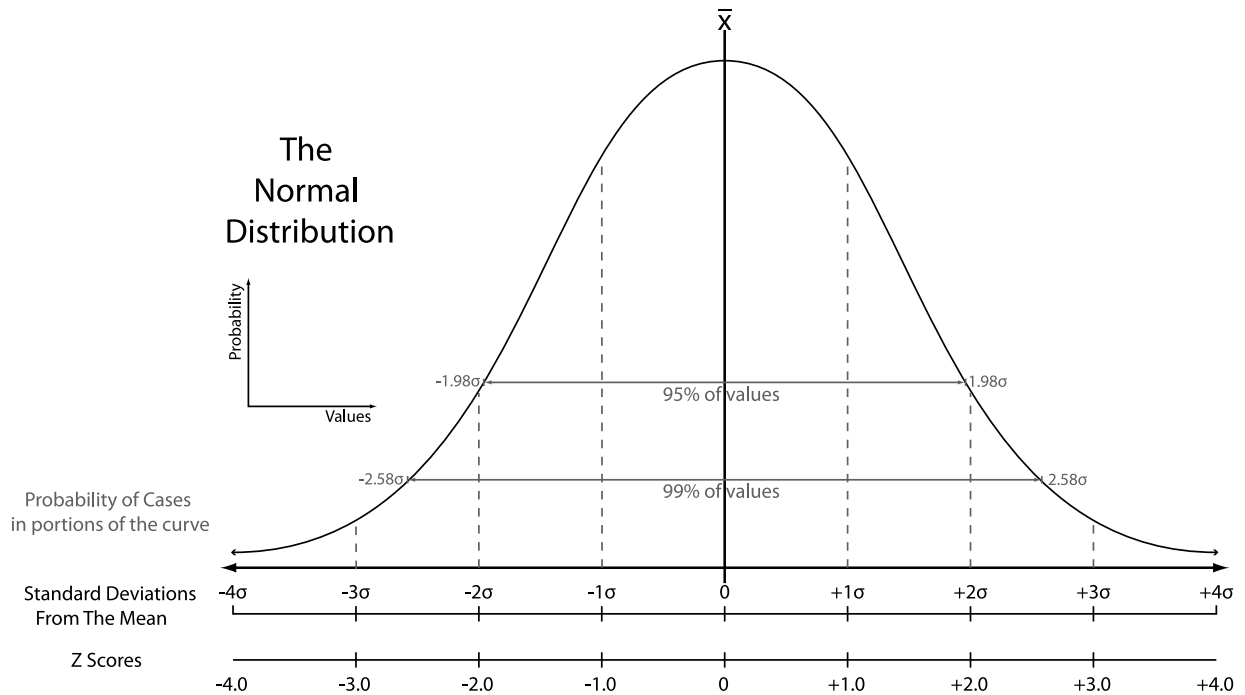


FIGURE 5.11: The Normal distribution.

5.5 SUMMARY

In this chapter, two novel land-cover change detection methods were proposed. The first method models an NDVI time-series as a triply modulated cosine function and estimates the mean, amplitude and phase for each time-increment using an EKF. A change index was derived by comparing each pixel's mean and amplitude parameters with that of its neighboring pixels, effectively considering the center pixel of a 3×3 grid of pixels. The threshold that determined whether the change index associated with each pixel should be classified as change or no-change was determined by means of land-cover change simulation.

The second method that was proposed is a temporal ACF change detection method. This method exploits the non-stationary property that is typical of a time-series of a pixel that undergoes land-cover change by considering the temporal ACF of the time-series. A change metric is defined by considering an ACF band and lag combination. The most appropriate band, lag and threshold selection is performed using a no-change and simulated change dataset.

For comparison, the NDVI differencing method proposed in [17] is also discussed. The performance of all three methods are evaluated on two study areas in South Africa, the results of which are presented in the following chapter.